Journal of Catalysis 390 (2020) 206–212

Contents lists available at ScienceDirect

Journal of Catalysis

journal homepage: www.elsevier.com/locate/jcat

Understanding the generation of long-chain hydrocarbons from CO_2 and water using cobalt nanostructures and light

Chunzheng Wu [a,b], Xinxin Xing [a,b], Guang Yang [c], Tian Tong [b], Zhiming M. Wang [a,*], Jiming Bao [b,c,*]

[a] Institute of Fundamental and Frontier Sciences, University of Electronic Science and Technology of China, Chengdu 610054, China
[b] Department of Electrical & Computer Engineering, University of Houston, Houston, TX 77204, USA
[c] Materials Science & Engineering, University of Houston, Houston, TX 77204, USA

ARTICLE INFO

Article history:
Received 29 May 2020
Revised 26 July 2020
Accepted 2 August 2020
Available online 12 August 2020

Keywords:
Photothermal
CO_2 reduction
Cobalt
Long-chain hydrocarbons
C2+ alkanes
Galvanic replacement
Deactivation

ABSTRACT

The production of long-chain hydrocarbons from CO_2 and water using solar light is a big challenge for the catalysis society. Cobalt nanostructures have been reported to catalyze the production of C3-C15 alkanes in a cobalt-water-CO_2 three-phase system under white light, yet the proposed photocatalytic mechanism still lacks evidence. In this work, cobalt micro- and nanostructures with different sizes and morphologies are used as model catalysts to reproduce this reaction. Despite different activity, selectivity and stability, the catalysts are found to follow the same reaction mechanism: a CO_2 assisted galvanic replacement reaction to produce H_2 followed by a thermal catalytic CO_2 hydrogenation to produce alkanes; meanwhile, the Co catalysts are gradually but inevitably converted to $CoCO_3$, leading to a slow deactivation. The low concentration of the in-situ formed H_2 favors the growth of C2+ alkanes. The incident light drives the reaction by heating the catalyst, rather than providing plasmonic hot electrons for CO_2 reduction.

1. Introduction

The production of petroleum or diesel-like long-chain hydrocarbons from CO_2, water and solar energy is really a dream of the catalysis society [1]. Usually, such big molecules (e.g. C3+) can hardly be obtained by a photocatalytic or electrocatalytic CO_2 reduction due to the kinetic limit [2–6], while the modified Fischer-Tropsch synthesis (with CO_2 as the reactant) may work but must be carried out at high temperatures with H_2 [7–9]. In the last decade, a few researchers have attempted this challenging synthesis by using Co as the catalyst. Wang et al. were the first to report a nature-like photosynthesis with femtosecond laser induced Co nanostructures in 2009 [10] and 2011 [11]. They claimed that H_2O and CO_2 were respectively disassociated to H_2 or H atoms (at excited states) and CO (at excited states) on Co due to the local strong electrical field around the tips. These activated molecules were then converted to long-chain hydrocarbons by Co nanostructures with an incredibly high production rate (*i.e.* above 50 ml/g/h liquid/solid hydrocarbons). Five years later, Chanmanee et al. made a similar design by using a Co/TiO_2 catalyst [12], but the reaction was proposed to be driven by both photo-excited electrons and thermal energy: the photo-excited electrons from TiO_2 under UV light were injected into the Co nanoparticles and reduced the adsorbed CO_2 to CO and adsorbed water to H_2 or H atoms, then the Co nanoparticles catalyzed a Fischer-Tropsch-like process at above 160 °C to yield long chain molecules. Unfortunately, their hydrocarbon products were proven to come from carbon impurities rather than CO_2 [12], and the paper was retracted by the authors about two years later. In contrast, Wang et al. published a follow-up paper this year using Co nanostructures from acid etching to extend their mechanism [13]. In this paper, they ruled out the interference of carbon impurities by using ^{13}C isotope labeling and offered a theoretical explanation of the surface plasmonic effect, *i.e.* the local field enhancement and hot electron generations, by employing density-functional theory (DFT) calculations.

Inspired by the new findings of Wang et al., we tried to gain more understandings of this reaction, especially the correlation between the plasmonic effect and the production of long-chain hydrocarbons, from the experimental side. We synthesized cobalt catalysts with different sizes and morphologies, and obtained long-chain hydrocarbons. However, X-ray diffraction (XRD), scanning electron microscope (SEM), Fourier-transform infrared spectroscopy (FTIR), combined with catalytic tests in different conditions revealed a totally different mechanism: the production of alkanes is a thermal CO_2 hydrogenation process with no evident contribution from photocatalytic effect. These reactions happen

* Corresponding authors.
E-mail addresses: zhmwang@uestc.edu.cn (Z.M. Wang), jbao@uh.edu (J. Bao).

https://doi.org/10.1016/j.jcat.2020.08.001
0021-9517/

generally on all Co samples, despite small influence of their sizes and morphologies.

2. Results and discussion

2.1. Cobalt catalysts

Co nano-micro-structures with different sizes and morphologies were prepared by using chemical reduction or acid etching methods [13,14]. Fig. 1a shows Co nanospheres (NSs) with a diameter of 30–60 nm. Fig. 1b shows Co micro-leaves (MLs) with a size of 3–5 μm and with their surface highly structured at the nanoscale. Co microparticles with their surfaces decorated by nanoflakes (MPNFs) were also prepared using commercial Co microparticles (MPs) with a large size (50–100 μm) and smooth surface (as shown in Fig. 1c). The obtained nanoflakes in Fig. 1d display a size of ~500 nm and a thickness of <50 nm. XRD in Fig. 1e roughly shows a face centered cubic (FCC) structure for Co NSs with no evident hexagonal close packed (HCP) phase. The XRD peaks are broad and weak due to the small size and poor crystallinity. The small peak at around 2θ = 46° was possibly from Co_2B [15,16], which usually forms in the reaction between Co^{2+} and $NaBH_4$ [16]. In contrast, Co MLs show clearly a HCP dominated structure with a trace FCC phase. The commercial MPs, either with or without nanoflakes, show a mixture of FCC and HCP phases, the same with Wang et al. [13] XPS of Co MLs in Fig. 1f displays strong signals of CoO (with satellites at 803.0 eV and 787.0 eV) [17] and a tiny peak of metallic Co (at 777.9 eV) [18]. It suggests that the surface of cobalt MLs is passivated by a thin layer of CoO (<5 nm) when exposed to air, while the core is still metallic, consistent with previous reports [11,13]. Such CoO layers protect the Co metal from oxidation.

2.2. Catalytic performance

C2+ alkanes have been successfully reproduced by Co NSs, MLs, and MPNFs in a glass batch reactor with CO_2 and water and irradiated by a halogen lamp (setup shown in Fig. S1). Taking Co MLs as an example, Fig. S2a shows that a significant amount of H_2 and straight-chain alkanes (C1–C11) and trace branched alkanes were detected in the gas phase after 20 h of irradiation. Analysis of the liquid/solid products, extracted by dichloromethane (CH_2Cl_2), also confirmed the presence of C6-C16 straight-chain alkanes as shown in Fig. S2b. The long-chain products are comparable with the latest

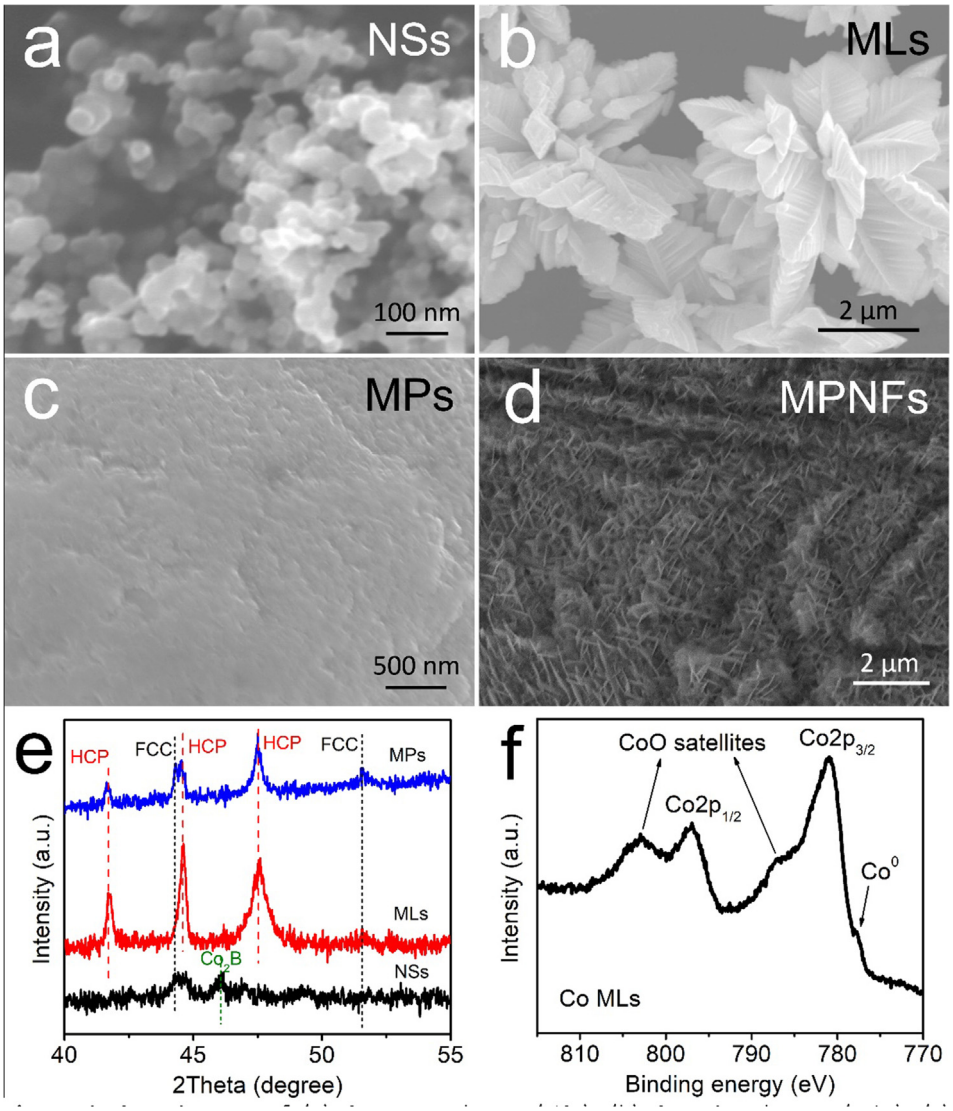

Fig. 1. SEM images of (a) Co nanospheres (NSs), (b) Co micro-leaves (MLs), (c) commercial Co microparticles (MPs) and (d) Co microparticles decorated with nanoflakes (MPNFs). (e) XRD patterns of Co NSs, MLs and MPs. (f) XPS results of Co MLs.

report of Wang et al. [13] No alkenes, alcohols, or CO was detected. For the convenience of analysis, only C1–C6 straight-chain alkanes in the gas phase were counted in the calculation of activity and selectivity. According to Fig. 1a and b, the activity and selectivity showed a trend that was related to the size and surface area of the Co catalysts. Co NSs with the smallest size and the largest surface area (*i.e.* 16.8 m^2/g) showed the highest conversion rate of CO_2 (*i.e.* 4.7 μmol/g/h) that was 2.7 times of MLs (*i.e.* 1.8 μmol/g/h, its surface area is 5.0 m^2/g) and two orders of magnitude higher than that of MPNFs (*i.e.* 0.02 μmol/g/h, its surface area is 0.7 m^2/g); meanwhile, the H_2 production follows the same trend as shown in Fig. 2a. On the other hand, Co NSs exhibited a lower selectivity to CH_4 (*i.e.* 51%) than MLs (*i.e.* 68%) and MPs (*i.e.* 77%). Despite 10 times more catalyst (*i.e.* 3 g) was used for MPNFs, it produced negligible alkanes compared to Co MLs and Co NSs (Fig. 2a) due to the super large size (50–100 μm) and small surface area. Apart from these factors, the difference in morphology, crystal structure, and composition may also affect the activity and selectivity, but it is not the scope of the current research.

Using Co MLs as the catalyst, the effect of the Co/H_2O ratio was studied. In the first set of experiments in Fig. 2c, 300 mg of Co was mixed with different amount of water (e.g. 0.3–1.5 ml) to tune the environment around it. Consistent with previous observation of Wang et al., the reaction with a solid–liquid-gas contact (0.5 ml of water) significantly outperformed the ones with solid–gas contact (0.3 ml of water) and solid–liquid contact (1.5 ml of water) [10,11,13]. In the second step, we changed the amount of Co catalyst while keeping the water and the area of Co that spread on the reactor. Surprisingly, the CO_2 conversion rate normalized by the area of light irradiation increased continuously, while the ones normalized by mass was almost constant (as shown in Fig. 2d). It suggested that the reaction rate was determined by the amount of catalyst, rather than the light irradiation area. In other words, the Co particles beneath the top surface were also participating in the CO_2 conversion reaction, which is against the basic principle of photochemistry. Fig. 2c and d shows that the selectivity to CH_4 varies gently between 60% and 70% with a same trend of the H_2O/CO_2 ratio, while H_2 has a similar trend with the conversion rate of CO_2.

Control experiments in Ar and in dark were carried out to verify this reaction. When CO_2 was replaced by Ar while keeping the other conditions, no hydrocarbon was detected as shown in Fig. 3a, confirming that CO_2 was the carbon source. However, neither H_2 nor O_2 was detected, suggesting that H_2 was not produced through the photocatalytic water splitting. Reaction with CO_2 and water in dark was then performed and the temperature of the catalyst was kept at about 120 °C by using different external heaters (*i.e.* a heating plate or an infrared heat emitter). As shown in Fig. 3, identical hydrocarbons and H_2 were produced under the infrared heat emitter (*i.e.* in dark) and the halogen lamp (*i.e.* under light). It clearly demonstrates a non-photochemistry nature of this reaction, which is completely different from the surface plasmon induced photocatalysis as proposed by Wang et al. [13]. The heat provided by the incident light (*i.e.* through a photothermal process) and by the heat emitter showed no difference in driving this reaction. When using a heating plate below the reactor, the reaction occurred as well but with some difference in the activity and selectivity (shown in Fig. S3). It was caused by the unsteady heating as well as the opposite temperature gradients (*i.e.* heat from the bottom).

2.3. CO_2 assisted production of H_2

With the above findings, the question becomes how the thermal/photothermal energy contributed to the production of H_2 and alkanes? Experiments were designed to discover the production of H_2 in dark. Typically, 100 mg of Co MLs were mixed with 0.5 ml of water at room temperature in a 48 ml vial and purged with pure CO_2, Ar, or air before sealing it. Fig. 4a shows that H_2 was continuously produced in CO_2 but not in the other two atmospheres, identical to the above control experiment at 120 °C. The

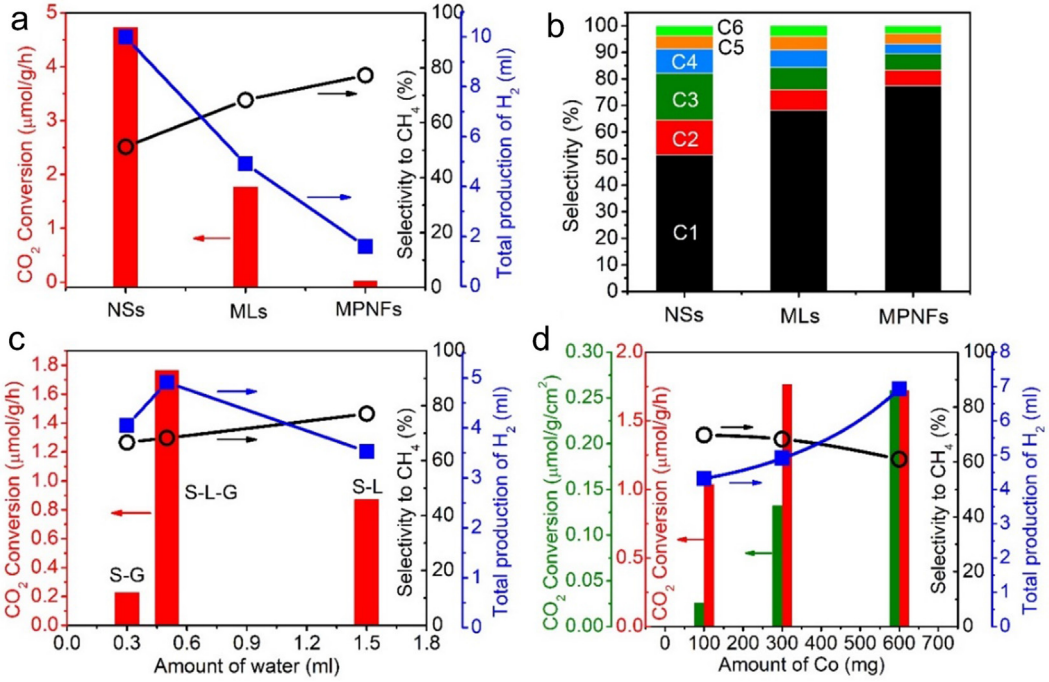

Fig. 2. A comparison of Co nanospheres (NSs), micro-leaves (MLs) and Co microparticles decorated with nanoflakes (MPNFs) in terms of (a) the rate of CO_2 conversion, the selectivity to CH_4, the total production of H_2, and (b) the detailed selectivity to C1–C6 alkanes. (c) The effect of water and the catalyst-environment interface on the catalytic performance. Solid-gas (S-G), solid–liquid-gas (S-L-G), and solid–liquid (S-L) interfaces were created when using 0.3, 0.5, and 1.5 ml of water, respectively. (d) The effect of the amount of catalyst on the activity and selectivity. The reaction rate of CO_2 was normalized either by the mass or by the irradiation area.

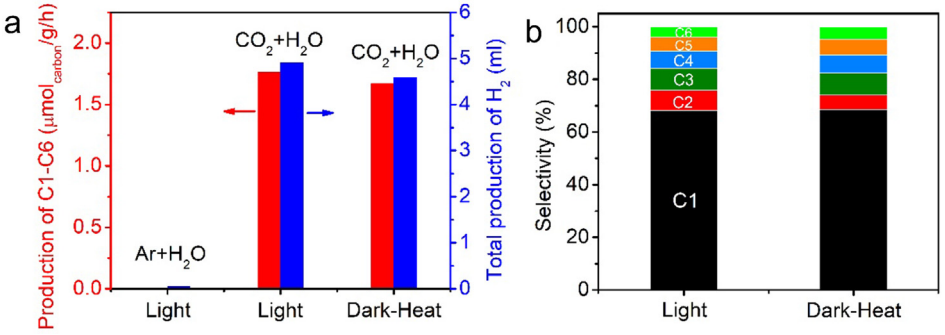

Fig. 3. (a) The production of C1–C6 and H_2 and (b) the selectivity of C1–C6 in light (under a halogen lamp) and in dark (under an infrared heat emitter).

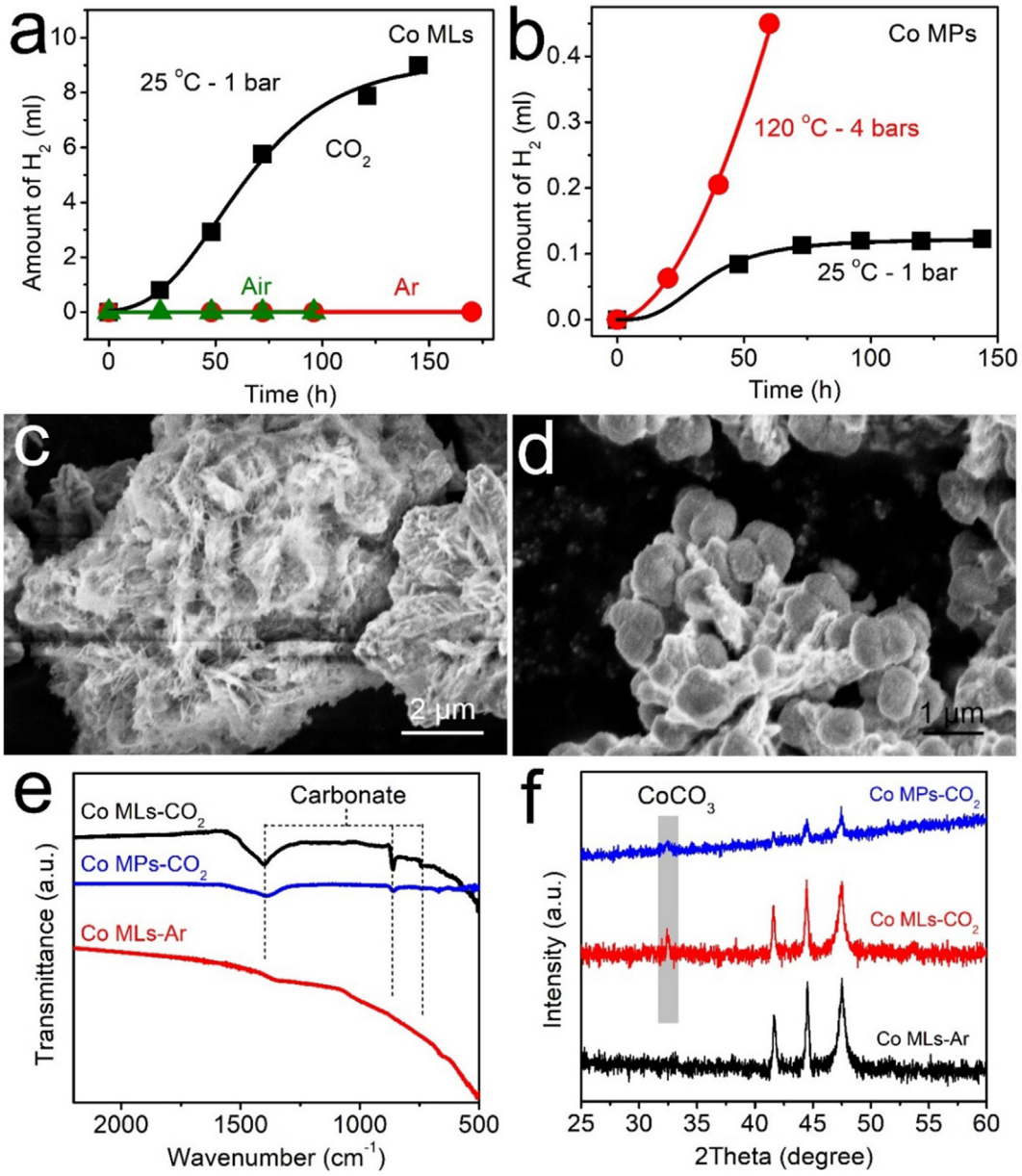

Fig. 4. (a) The production of H_2 with Co micro-leaves (MLs) under different atmospheres. Conditions: 100 mg of Co MLs was mixed with 0.5 ml of water at 25 °C in a 48 ml vial. The vial was purged with pure CO_2, pure Ar, or air, then sealed and placed in dark. The concentration of H_2 was analyzed every day. (b) The production of H_2 with commercial Co MPs at different conditions. SEM images of Co MLs after storing in H_2O with (c) pure Ar or (d) pure CO_2 for 1 week. (e) FTIR spectra and (f) XRD patterns of Co MLs and Co MPs in H_2O with pure CO_2 or Ar for 1 week.

Co MLs after storing in CO_2 and Ar for one week were compared. SEM in Fig. 4c shows that Co MLs in Ar maintained the microleaves shape although their surface has been seriously contaminated by nanosheet or nanoneedle-like species. In contrast, Fig. 4d shows that Co MLs in CO_2 have been completely transformed to a micro-mushroom shape. FTIR in Fig. 4e and XRD in Fig. 4f further prove the emergence of $CoCO_3$ phase after storing in CO_2, but not in Ar. This correlation indicates that CO_2 functioned as a reactant, rather than a catalyst, in the production of H_2.

Theoretically, the galvanic replacement between Co and water to produce H_2 (*i.e.* $Co + H_2O \rightarrow CoO + H_2$) is thermodynamically feasible at room temperature (according to the thermodynamic equilibriums in Fig. S4), although it may be kinetically limited by the low temperature and pressure, small surface area of Co, and low concentration of H^+. As an acidic gas, CO_2 was supposed to promote the reaction in the forward direction by forming a stable product $CoCO_3$ (e.g. $Co + H_2O + CO_2 \rightarrow CoCO_3 + H_2$). To confirm the generality of this reaction, the commercial Co MPs with large size and smooth surface (50–100 μm, used by Wang et al. [10,11,13]) were also tested. As shown in Fig. 4b, e and f, both H_2 and $CoCO_3$ were produced, although the reaction rate was much lower due to the limited surface area. Increasing the temperature and CO_2 pressure to the testing condition (e.g. 120 °C and 4 bars) dramatically boosted the galvanic replacement.

2.4. CO_2 hydrogenation reaction

With the noticeable production of H_2 from the galvanic replacement in the testing condition (e.g. 120 °C and 4 bars), it is questionable whether H_2O or H_2 is H source for the alkanes. Thermodynamic equilibriums in Fig. S5 indicate that CO_2 and H_2O can never be converted to alkanes (through $CO_2 + H_2O \rightarrow C_nH_{2n+2} + O_2$) even at temperatures up to 1000 °C, in the absence of photocatalytic or electrocatalytic contribution. On the contrary, its reverse reactions, such as the combustion of methane [19,20] and volatile organic compounds (VOC) [21,22], are certainly available in thermal conditions. Thereby, we believe that water is not the direct reactant for the alkanes.

Experiments were designed to figure out if the *in-situ* formed H_2 was converted to alkanes or not. Reactions at 120 °C for different time periods (*i.e.* 5 h, 20 h, and 40 h) and reactions at different temperatures (*i.e.* 95 °C, 120 °C, and 158 °C) for 20 h were performed. The former experiment in Fig. 5a showed a normal increase of H_2 with reaction time, consistent with the test at room temperature in Fig. 4a. The H_2 concentration of the latter experiment in Fig. 5b, however, showed a volcano shaped trend with the increase of temperature. Considering that the galvanic replacement should be both thermodynamically (thermodynamic equilibriums shown in Fig. S4) and kinetically enhanced at elevated temperatures, the lower concentration of H_2 at 158 °C than that at 120 °C suggested a consumption of H_2 during this process. Considering also the much higher conversion rate of CO_2 at 158 °C (shown in Fig. 5b), we believe that H_2 was consumed by CO_2 to produce alkanes at the elevated temperatures. This proposed CO_2 hydrogenation process was further confirmed by directly testing in a mixture of H_2 and CO_2 with a volume ratio of 1/7. It was mimicking the final H_2/CO_2 ratio in the CO_2-H_2O system after 20 h of test at 120 °C. As a result, Fig. 5c and d shows similar selectivity of C1–C6 alkanes but with ~10 times higher amount compared to the CO_2-H_2O system. The identical distribution of products demonstrated that the gas phase hydrogenation was the real process that happening in the CO_2-H_2O system. The relatively lower activity of the CO_2-H_2O system was due to the blockage of the Co surface by water or $CoCO_3$.

Generally, the production of C2+ alkanes from CO_2 and H_2 is unusual for pure Co, which is known as a CO_2 methanation catalyst [23–25]. The contribution of plasmonic effect to the growth of carbon chains, as proposed by Wang et al. [13], has been ruled out by doing a series of tests in dark and under light. Fig. S6a and b show identical activity and selectivity in these two conditions, consistent with our CO_2-H_2O system as well as many previous reports of Co based catalysts for CO/CO_2 hydrogenation [26–28]. According to the literature, long-chain hydrocarbons can also be produced in dark through a tandem process that consists of a reverse water gas shift (RWGS, $CO_2 + H_2 \rightarrow CO + H_2O$) reaction and a Fischer-Tropsch synthesis process ($CO + H_2 \rightarrow C_xH_y + H_2O$) [7,26]. However, this mechanism is not true for our system due to lack of a RWGS catalyst (such as Pt [7], Fe [26], Cu [29]) and the absence of CO throughout the test. In fact, we found that by altering the H_2/CO_2 ratio in the gas phase from 1/7 to 3/1, the selectivity to C2+ alkanes dropped dramatically from ~35% to ~3% (shown in Fig. 5e). It meant that the high atomic ratio of C/H on Co favored the carbon–carbon coupling [8,30].

2.5. Stability

Despite the production of alkanes, this process is not sustainable due to the chemical reaction happened on Co catalyst. Figs. S7–9 show significant structural, morphological, and compositional changes for all the Co MLs, NSs, MPNFs, and MPs after the test. The surface CoO layer on MLs failed to protect the Co metal from galvanic replacement reaction since CoO reacted with CO_2 easily (evidence shown in Fig. S10). Reactions on the smooth and nanostructure-free MPs also created abundant $CoCO_3$ microislands on their surface (as shown in Fig. S9b and c). This transformation is thermodynamically inevitable under the testing condition, and is kinetically accelerated by lowering the size, creating nanostructures, or increasing the surface area of Co. Therefore, the reported good stability of Co nanoflakes under the identical testing conditions by Wang et al. [13] is doubtful.

The galvanic replacement induced consumption of Co MLs in each cycle was calculated to be ~15.8 mg based on the average amount of H_2 produced. Thus, 300 mg of Co MLs allowed about 19 cycles of tests if keeping the same conversion rate of Co. Using more catalysts (such as 600 mg or 3 g) would further prolong and smooth out the deactivation. On the other hand, the activity was more sensitive to the configuration of Co and $CoCO_3$, rather than the consumption of Co. When the formed $CoCO_3$ was mixed with Co NSs as shown in Fig. S8d, rather than coating on the surface (like the Co MLs shown in Fig. S7d), the catalyst exhibited a relatively stable activity with no evident decline in four tests (Fig. S8a). Therefore, cyclability tests with limited cycles (for example ≤4 cycles) may send out misleading information about their stability

2.6. The overall mechanism

The proposed mechanism is shown in Scheme 1. The "magic" production of alkanes from water and CO_2 under light is neither a photocatalytic reaction nor a sole thermal catalytic reaction. No evidence of plasmonic effect has been found. In fact, the plasmonic behavior of Co has been rarely reported so far [31–33]. Bhatta et al. claimed that only the monodispersed Co colloids (~9 nm) exhibit a plasmonic absorption at UV region, and any aggregation of the Co particles vanishes the plasmon resonance dramatically due to electron scattering with spin flip in the presence of second magnetic particles [33]. Based on their finding, it is theoretically not possible for Co powders to generate surface plasmon resonance due to the stack of particles. The contribution of the 5% UV in solar light has also been experimentally ruled out by simultaneously irradiating the catalyst with a halogen lamp (visible-NIR light) and an UV lamp (~400 nm). As shown in Fig. S11, identical activity and selectivity were observed when keeping the same temperature.

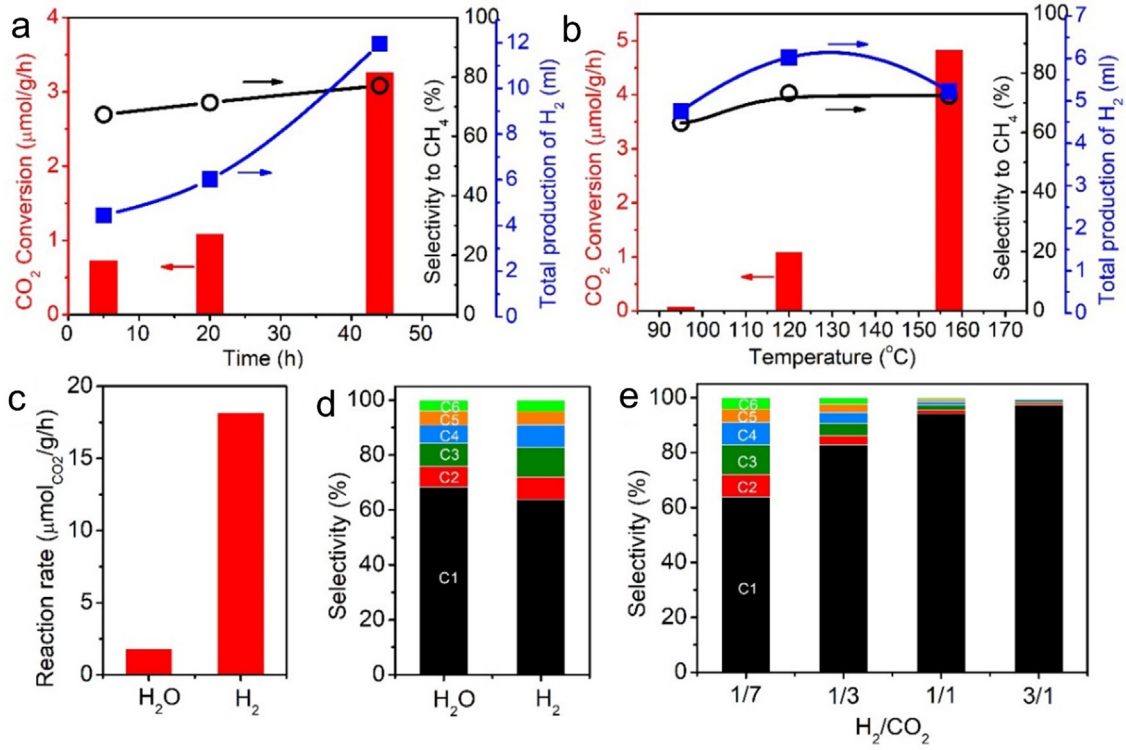

Fig. 5. The effects of (a) reaction time and (b) reaction temperature on the activity and selectivity. Comparison of the (c) activity and (d) selectivity of the CO_2-H_2O and CO_2-H_2 systems. Conditions: 300 mg of Co MLs was mixed with 0.5 ml of water and 4 bars of CO_2 or 0.5 bar of H_2 and 3.5 bar of CO_2, then reacted at 120 °C for 20 h under light. (e) The effect of the H_2/CO_2 ratio on the selectivity to C1–C6 alkanes.

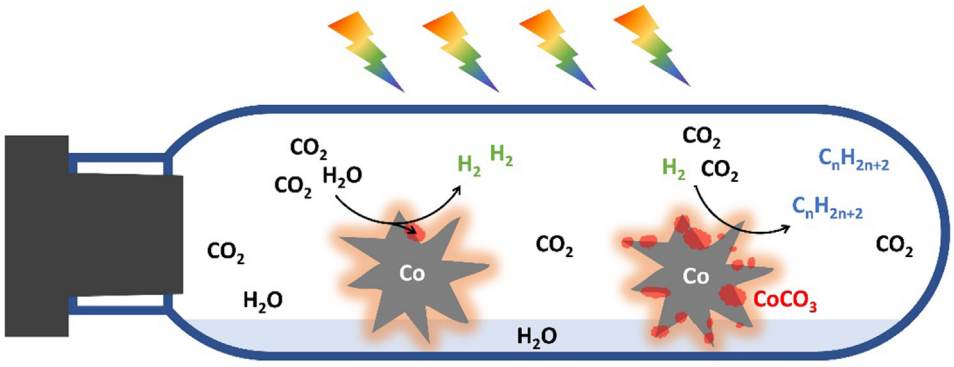

Scheme 1. Mechanism of the photothermal production of alkanes (*i.e.* C_nH_{2n+1}, n = 1–16) in a Co-CO_2-water three-phase system under light irradiation. The left particle shows the CO_2 induced galvanic replacement between Co and H_2 to produce H_2 and $CoCO_3$ while the right particle shows the subsequent gas-phase CO_2 hydrogenation reaction on Co to produce alkanes. This reaction is driven by the thermal energy from the UV–Vis-NIR light. Co was continuously converted to $CoCO_3$.

In contrast to the plasmonic effect, the contribution of photothermal energy to the production of alkane is quite evident. Under the light irradiation, Co catalysts are efficiently heated thanks to their full absorption of UV–Vis-NIR light. The production of alkanes consists of two steps as shown in Scheme 1. First, H_2 is produced through a galvanic replacement between Co and H_2O with the assistance of CO_2. This reaction becomes significant with increasing temperature, increasing CO_2 pressure and downsized Co catalyst. Second, a gas phase CO_2 hydrogenation reaction takes place on the exposed Co metal driven by the photothermal energy. The relatively low concentration of H_2 favors the carbon–carbon coupling to form long-chain alkanes.

Due to a good performance in carbon–carbon coupling in the Fischer-Tropsch synthesis, Co was selected by both Chanmanee et al. [12] and Wang et al. [10,11,13] to synthesize long-chain hydrocarbon from CO_2 and water. However, its poor stability in such conditions has not been noticed. In fact, research on Fischer-Tropsch has shown many deactivation cases that caused by oxidation of Co metal by the in-situ formed water [34–36]. Our research shows that concentrated CO_2 will largely accelerate the Co oxidation and form inactive $CoCO_3$ in the presence of water at elevated temperatures. Therefore, Co is not a good candidate for such applications.

3. Conclusion

We have successfully reproduced the long-chain alkanes starting from CO_2 and water by using various Co nano-microstructures. However, no evidence of the surface plasmon induced photocatalytic process has been observed. Instead, we found it

occur through a galvanic replacement chemical reaction followed by a gas phase thermal catalytic CO_2 hydrogenation reaction. Alkanes were produced in a CO_2 rich and H_2 lean atmosphere at the cost of the Co metals. Based on this finding, the stability of cobalt in a CO_2 rich aqueous environment is the main challenge for this application, and structure designs by integrating proper light harvesters and electron donors are the potential solutions in future.

Declaration of Competing Interest

The authors declare that they have no known competing financial interests or personal relationships that could have appeared to influence the work reported in this paper.

Acknowledgements

J. Bao acknowledges support from the Robert A. Welch Foundation (E-1728). We acknowledge Dr. Kehley Davies, Prof. David K. Ryan and Prof. Mengyan Shen from University of Massachusetts Lowell for sharing their experience in synthesizing and testing the cobalt samples. We acknowledge Dr. Qingbin Yuan and Zhaoyang Chen for measuring BET surface areas.

Appendix A. Supplementary material

Supplementary data to this article can be found online at https://doi.org/10.1016/j.jcat.2020.08.001.

References

[1] O.K. Varghese, M. Paulose, T.J. LaTempa, C.A. Grimes, High-rate solar photocatalytic conversion of CO_2 and water vapor to hydrocarbon fuels, Nano Lett. 9 (2009) 731–737.
[2] H. Park, H.-H. Ou, A.J. Colussi, M.R. Hoffmann, Artificial photosynthesis of C1–C3 hydrocarbons from water and CO_2 on titanate nanotubes decorated with nanoparticle elemental copper and CdS quantum dots, J. Phys. Chem. A 119 (2015) 4658–4666.
[3] Z. Weng, J. Jiang, Y. Wu, Z. Wu, X. Guo, K.L. Materna, W. Liu, V.S. Batista, G.W. Brudvig, H. Wang, Electrochemical CO_2 reduction to hydrocarbons on a heterogeneous molecular Cu catalyst in aqueous solution, J. Am. Chem. Soc. 138 (2016) 8076–8079.
[4] A. Liu, M. Gao, X. Ren, F. Meng, Y. Yang, L. Gao, Q. Yang, T. Ma, Current progress in electrocatalytic carbon dioxide reduction to fuels on heterogeneous catalysts, J. Mater. Chem. A 8 (2020) 3541–3562.
[5] Q. Chen, X. Chen, M. Fang, J. Chen, Y. Li, Z. Xie, Q. Kuang, L. Zheng, Photo-induced Au–Pd alloying at TiO2 101 facets enables robust CO2 photocatalytic reduction into hydrocarbon fuels, J. Mater. Chem. A 7 (2019) 1334–1340.
[6] C. Li, X. Tong, P. Yu, W. Du, J. Wu, H. Rao, Z.M. Wang, Carbon dioxide photo/electroreduction with cobalt, J. Mater. Chem. A 7 (2019) 16622–16642.
[7] C. Xie, C. Chen, Y. Yu, J. Su, Y. Li, G.A. Somorjai, P. Yang, Tandem catalysis for CO_2 hydrogenation to C2–C4 hydrocarbons, Nano Lett. 17 (2017) 3798–3802.
[8] Z. He, M. Cui, Q. Qian, J. Zhang, H. Liu, B. Han, Synthesis of liquid fuel via direct hydrogenation of CO_2, Proc. Natl. Acad. Sci. 116 (2019) 12654.
[9] L. Guo, J. Sun, Q. Ge, N. Tsubaki, Recent advances in direct catalytic hydrogenation of carbon dioxide to valuable C2+ hydrocarbons, J. Mater. Chem. A 6 (2018) 23244–23262.
[10] C. Wang, M. Shen, H. Huo, H. Ren, F. Yan, M. Johnson, Nature-like photosynthesis of water and carbon dioxide with femtosecond laser induced self-assembled metal nanostructures, Int. J. Mod. Phys. B 23 (2009) 5849–5857.
[11] C. Wang, M. Shen, H. Huo, H. Ren, M. Johnson, Using metal nanostructures to form hydrocarbons from carbon dioxide, water and sunlight, AIP Adv. 1 (2011) 042124.
[12] W. Chanmanee, M.F. Islam, B.H. Dennis, F.M. MacDonnell, Solar photothermochemical alkane reverse combustion, Proc. Natl. Acad. Sci. 113 (2016) 2579.
[13] C. Wang, H. Ren, M. Zeng, Q. Zhu, Q. Zhang, Z. Kan, Z. Wang, M. Shen, M.J. Thalavitiya Acharige, M. Ruths, D.K. Ryan, G. Li, G. Kolesov, E. Kaxiras, E. Mazur, Low-cost visible-light photosynthesis of water and adsorbed carbon dioxide into long-chain hydrocarbons, Chem. Phys. Lett. 739 (2020) 136985.
[14] K. Davies, D.K. Ryan, Selective production of naphthalene from methanol by photocatalysis on nanostructured cobalt particles, Catal. Today 350 (2020) 142–148.
[15] I. Campos-Silva, D. Bravo-Bárcenas, H. Cimenoglu, U. Figueroa-López, M. Flores-Jiménez, O. Meydanoglu, The boriding process in CoCrMo alloy: Fracture toughness in cobalt boride coatings, Surf. Coat. Technol. 260 (2014) 362–368.
[16] G.N. Glavee, K.J. Klabunde, C.M. Sorensen, G.C. Hadjapanayis, Borohydride reductions of metal ions. A new understanding of the chemistry leading to nanoscale particles of metals, borides, and metal borates, Langmuir 8 (1992) 771–773.
[17] L. Liao, Q. Zhang, Z. Su, Z. Zhao, Y. Wang, Y. Li, X. Lu, D. Wei, G. Feng, Q. Yu, X. Cai, J. Zhao, Z. Ren, H. Fang, F. Robles-Hernandez, S. Baldelli, J. Bao, Efficient solar water-splitting using a nanocrystalline CoO photocatalyst, Nat. Nanotechnol. 9 (2013) 69.
[18] P. Bazylewski, D.W. Boukhvalov, A.I. Kukharenko, E.Z. Kurmaev, A. Hunt, A. Moewes, Y.H. Lee, S.O. Cholakh, G.S. Chang, The characterization of Co-nanoparticles supported on graphene, RSC Adv. 5 (2015) 75600–75606.
[19] J. Chen, H. Arandiyan, X. Gao, J. Li, Recent advances in catalysts for methane combustion, Catal. Surv. Asia 19 (2015) 140–171.
[20] P.J. Jodłowski, R.J. Jędrzejczyk, D. Chlebda, M. Gierada, J. Łojewska, In situ spectroscopic studies of methane catalytic combustion over Co, Ce, and Pd mixed oxides deposited on a steel surface, J. Catal. 350 (2017) 1–12.
[21] S. Li, D. Wang, X. Wu, Y. Chen, Recent advance on VOCs oxidation over layered double hydroxides derived mixed metal oxides, Chin. J. Catal. 41 (2020) 550–560.
[22] W. Pei, L. Dai, Y. Liu, J. Deng, L. Jing, K. Zhang, Z. Hou, Z. Han, A. Rastegarpanah, H. Dai, PtRu nanoparticles partially embedded in the 3DOM $Ce_{0.7}Zr_{0.3}O_2$ skeleton: Active and stable catalysts for toluene combustion, J. Catal. 385 (2020) 274–288.
[23] P. Riani, G. Garbarino, T. Cavattoni, F. Canepa, G. Busca, Unsupported cobalt nanoparticles as catalysts: Effect of preparation method on catalytic activity in CO_2 methanation and ethanol steam reforming, Int. J. Hydrogen Energy 44 (2019) 27319–27328.
[24] W. Li, X. Nie, X. Jiang, A. Zhang, F. Ding, M. Liu, Z. Liu, X. Guo, C. Song, ZrO_2 support imparts superior activity and stability of Co catalysts for CO_2 methanation, Appl. Catal. B 220 (2018) 397–408.
[25] T.A. Le, M.S. Kim, S.H. Lee, E.D. Park, CO and CO_2 methanation over supported cobalt catalysts, Top. Catal. 60 (2017) 714–720.
[26] G. Chen, R. Gao, Y. Zhao, Z. Li, G.I.N. Waterhouse, R. Shi, J. Zhao, M. Zhang, L. Shang, G. Sheng, X. Zhang, X. Wen, L.-Z. Wu, C.-H. Tung, T. Zhang, Alumina-supported CoFe alloy catalysts derived from layered-double-hydroxide nanosheets for efficient photothermal CO_2 hydrogenation to hydrocarbons, Adv. Mater. 30 (2018) 1704663.
[27] Z. Li, J. Liu, Y. Zhao, R. Shi, G.I.N. Waterhouse, Y. Wang, L.-Z. Wu, C.-H. Tung, T. Zhang, Photothermal hydrocarbon synthesis using alumina-supported cobalt metal nanoparticle catalysts derived from layered-double-hydroxide nanosheets, Nano Energy 60 (2019) 467–475.
[28] Z. Li, J. Liu, Y. Zhao, G.I.N. Waterhouse, G. Chen, R. Shi, X. Zhang, X. Liu, Y. Wei, X.-D. Wen, L.-Z. Wu, C.-H. Tung, T. Zhang, Co-based catalysts derived from layered-double-hydroxide nanosheets for the photothermal production of light olefins, Adv. Mater. 30 (2018) 1800527.
[29] Z. Shi, H. Yang, P. Gao, X. Li, L. Zhong, H. Wang, H. Liu, W. Wei, Y. Sun, Direct conversion of CO_2 to long-chain hydrocarbon fuels over K–promoted CoCu/TiO_2 catalysts, Catal. Today 311 (2018) 65–73.
[30] W. Li, G. Zhang, X. Jiang, Y. Liu, J. Zhu, F. Ding, Z. Liu, X. Guo, C. Song, CO_2 Hydrogenation on unpromoted and M-promoted Co/TiO_2 catalysts (M = Zr, K, Cs): Effects of crystal phase of supports and metal-support interaction on tuning product distribution, ACS Catal. 9 (2019) 2739–2751.
[31] S.M. Hamidi, B. Mosaeii, M. Afsharnia, A. Aftabi, M. Najafi, Magneto-plasmonic study of aligned Ni, Co and Ni/Co multilayer in polydimethylsiloxane as magnetic field sensor, J. Magn. Magn. Mater. 417 (2016) 413–419.
[32] S. Shukla, N.K. Sharma, V. Sajal, Theoretical study of surface plasmon resonance-based fiber optic sensor utilizing cobalt and nickel films, Braz. J. Phys. 46 (2016) 288–293.
[33] H.L. Bhatta, A.E. Aliev, V.P. Drachev, New mechanism of plasmons specific for spin-polarized nanoparticles, Sci. Rep. 9 (2019) 2019.
[34] M. Wolf, H. Kotzé, N. Fischer, M. Claeys, Size dependent stability of cobalt nanoparticles on silica under high conversion Fischer-Tropsch environment, Faraday Discuss. 197 (2017) 243–268.
[35] J. Yang, X. Fang, Y. Xu, X. Liu, Investigation of the deactivation behavior of Co catalysts in Fischer-Tropsch synthesis using encapsulated Co nanoparticles with controlled SiO_2 shell layer thickness, Catal. Sci. Technol. 10 (2020) 1182–1192.
[36] M. Wolf, N. Fischer, M. Claeys, Capturing the interconnectivity of water-induced oxidation and sintering of cobalt nanoparticles during the Fischer-Tropsch synthesis in situ, J. Catal. 374 (2019) 199–207.